# Single-Mask Phase Imaging Micro-Computed Tomography with Multi-Contrast Images and Single-Shot per Projection Angle

Jingcheng Yuan<sup>a</sup>, Ian Harmon<sup>a</sup>, JC Rodriguez Luna<sup>a</sup>, and Mini Das<sup>a,b</sup>

<sup>a</sup>Department of Physics, University of Houston, 3507 Cullen Blvd, Houston, TX 77204, USA <sup>b</sup>Department of Biomedical Engineering, University of Houston, 3517 Cullen Blvd, Houston, TX 77204, USA

## ABSTRACT

X-ray phase contrast imaging (XPCI) holds immense promise for enhancing contrast and visibility in medical imaging, as it harnesses the phase information within X-ray wavefront to reveal intricate structures within soft tissues. Among the diverse techniques available for x-ray phase contrast imaging, the single-mask phase contrast imaging method stands out for its notable benefits: heightened contrast levels, minimal system complexity demands, and the capacity to extract multi-modal information within a single shot. In this study, we introduce an X-ray phase contrast tomography system designed to deliver exceptional contrast for soft materials, along with the unique capability to retrieve absorption, differential phase, and phase images in a single shot per projection angle. Notably, our imaging setup circumvents the necessity for a highly coherent x-ray source, an ultra-high-resolution detector, or intricately fabricated x-ray gratings. Moreover, it exhibits substantial resilience towards alignment discrepancies and mechanical vibrations, contributing to its robust performance. While the methods would translate to all CT systems with the mask design available, we demonstrate our results in a benchtop system suitable for micro CT type imaging.

Keywords: X-ray phase contrast imaging, computed tomography, single mask phase imaging, micro CT

## 1. INTRODUCTION

X-ray projection imaging, which exploits variations in attenuation properties within the imaged object, is a widely employed technique in medical imaging of the human body. However, the utility of absorption-based X-ray images is constrained due to the relatively low attenuation exhibited by low-atomic-number materials, such as soft tissue.

When X-rays interact with objects, their intensity decreases due to object attenuation, and their phase is altered due to variations in the speed of light inside the object. Therefore, the object can be characterized by a complex refractive index given by:

$$n = 1 - \delta + i\beta \tag{1}$$

where the imaginary part is associated with attenuation and the real part is associated with phase. For most soft tissues, the value of  $\delta$  is typically several orders of magnitude higher than  $\beta$  for X-rays. Addressing the limitation of conventional X-ray imaging, X-ray phase-contrast imaging (PCI) has emerged as a promising approach for enhancing signal detection contrast within soft tissues. This innovative technique holds the potential to ameliorate the challenges posed by conventional absorption-based imaging<sup>1</sup>.<sup>2</sup>

The single-mask, which is developed by Krejci et al<sup>3</sup> based on double-mask edge-illumination set-up pioneered by Olivo's group<sup>4</sup>,<sup>5</sup> is known as one of the most advanced techniques of phase contrast imaging. Unlike traditional phase-contrast methods that require complex setups with multiple optical components, the single-mask method simplifies the process by incorporating just one additional optic into the beam path: the periodic absorption mask or grid. Positioned proximate to the object, the absorption mask resides between the source and the object, and the detector is positioned downstream of the sample at a distance, as illustrated in Fig. 1.

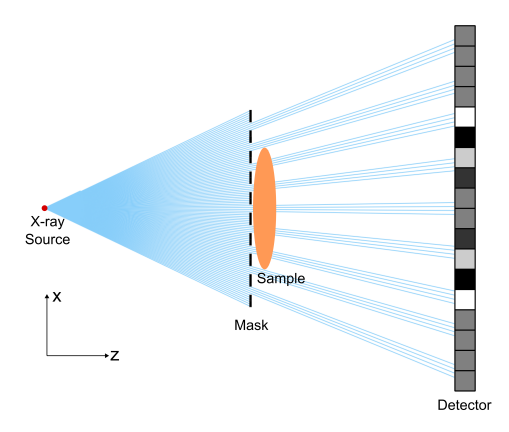


Figure 1: Schematic of single-mask x-ray phase contrast imaging system.

By virtue of the periodic absorption mask, the incident x-ray beam undergoes partitioning into a series of slender beamlets, with each beamlet meticulously aligned with the boundaries of detector pixels. In the absence of any sample within the beam path, a uniform distribution of illumination graces each detector pixel. However, upon the introduction of a sample into the beam, the wavefront undergoes distortion and the beamlets are refracted. Consequently, certain beamlets deviate from their original positions at the detector boundaries, resulting in a disparity in the intensities measured by adjacent pairs of pixels.

The key innovation of the single-mask method lies in its capability to extract both absorption and phase contrast information simultaneously from a single exposure. This distinguishes it from other methods such as propagation-based imaging and double-mask edge-illumination imaging. Unlike these methods, which either rely on oversimplified assumptions like the single-material assumption proposed by Paganin et al., require spectral information recessitate multiple exposures per projection angle to extract both absorption and phase components, the single-mask method offers a more straightforward and efficient approach to achieving multicontrast phase imaging.

Our previous study<sup>11</sup> shows that the x-ray intensity measured by the detector pixels can be written as the following formula based on transport-of-intensity equation (TIE):

$$I_n = w_e T_n (1 - L_n) + \alpha (-1)^n T_n D_n$$
(2)

where  $I_n$  is the intensity measured by the  $n^{th}$  detector pixel (in horizontal direction);  $T_n$  is the attenuation signal;  $L_n = \frac{z}{k} \nabla_{\perp}^2 \phi(x_n)$  is the Laplacian phase signal;  $D_n = \frac{z}{k} \partial_x \phi(x_n)$  is the gradient of phase;  $w_e$  and alpha is the effective opening width and contrast of the mask, respectively.

Following the retrieval technique based on our model, <sup>11</sup> one can the simultaneous extract absorption (with Laplacian phase signal) and differential phase contrast (DPC) image in a single exposure:

$$T_n(1 - L_n) \approx \frac{\bar{I}_n + \bar{I}_{n+1}}{2} \tag{3a}$$

$$D_n \approx (-1)^n \frac{w_e}{\alpha} \frac{\bar{I}_n - \bar{I}_{n+1}}{\bar{I}_n + \bar{I}_{n+1}}$$
(3b)

#### 2. METHOD

In our phase contrast tomography scan setup, we used a polychromatic microfocus x-ray tube (Hama-matsu L8121-03) operating with a focal spot of  $7\,\mu m$ . The tube voltage and current were 50 kV and  $190\,\mu A$  respectively. Both the source-to-mask distance and the mask-to-detector distance were maintained at approximately

Further author information: (Send correspondence to Mini Das) Mini Das.: E-mail: mdas@uh.edu, Telephone: +1 713-743-3539 60 cm. The object is placed on a rotation stage approximately 13 cm to the mask. We used the golden mask with the period of  $53\,\mu m$  manufactured by CREATV Microtech, with gold strips of  $100\,\mu m$  thick and  $33\,\mu m$  wide in each period.

The data acquisition was performed utilizing a Silicon Medipix3 photon-counting detector, <sup>12</sup> featuring a pixel size of 55 µm under charge summing mode. Photon counting detectors (PCDs) offer several advantages over traditional energy integrating detectors (EIDs) for X-ray imaging, including enhanced efficiency, superior spatial resolution, improved noise property, and the capability for multi-energy imaging, particularly in low-dose imaging scenarios. Despite its spectral capabilities, the detector was employed as an energy integrating detector with zero dark noise, as spectral information is not required for the single-mask method to extract both absorption and phase information. Prior to data acquisition, the detector underwent meticulous calibration and correction procedures based on our previous work<sup>13</sup>.<sup>14</sup>

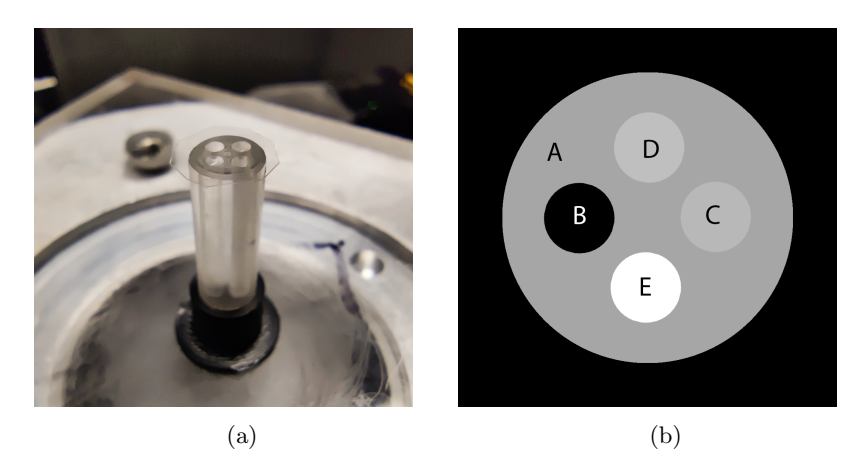


Figure 2: (a) Picture of the sample. (b) Diagram of the sample. The sample consists of PMMA (A), air (B), water (C), 10% aluminum nitrate (D), and 10% potassium iodide (E).

The sample utilized in our study was a poly(methyl methacrylate) (PMMA) cylinder, featuring a diameter of 6 mm. It contained four smaller 1.5 mm diameter holes, each filled with distinct materials: air, water, 10% aluminum nitrate, and 10% potassium iodide. To prevent evaporation during the measurement, the holes were sealed with small pieces of tape, as depicted in Fig. 2. Employing small-sized samples aimed to assess the contrast of minute structures within soft materials. A total of 360 frames were acquired during the CT scan, with each frame having a duration of 15 seconds. For each frame, the detector recorded an approximate count of 900 photons per pixel.

Before doing CT reconstruction, the first step is to retrieve the absorption and differential phase projections from the raw data using Eqn. (3a) and (3b). The examples of the retrieved absorption and differential phase projections are shown in Fig. 3. The reconstruction of projections was executed employing the method illustrated in Fig. 4.

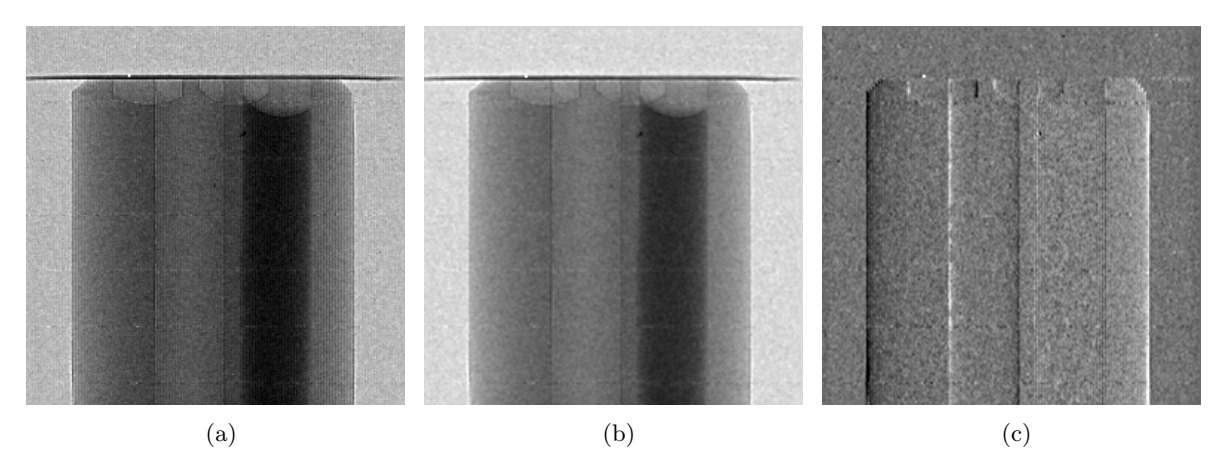


Figure 3: Example of (a) raw projection, (b) retrieved attenuation projection, and (c) retrieved differential phase projection.

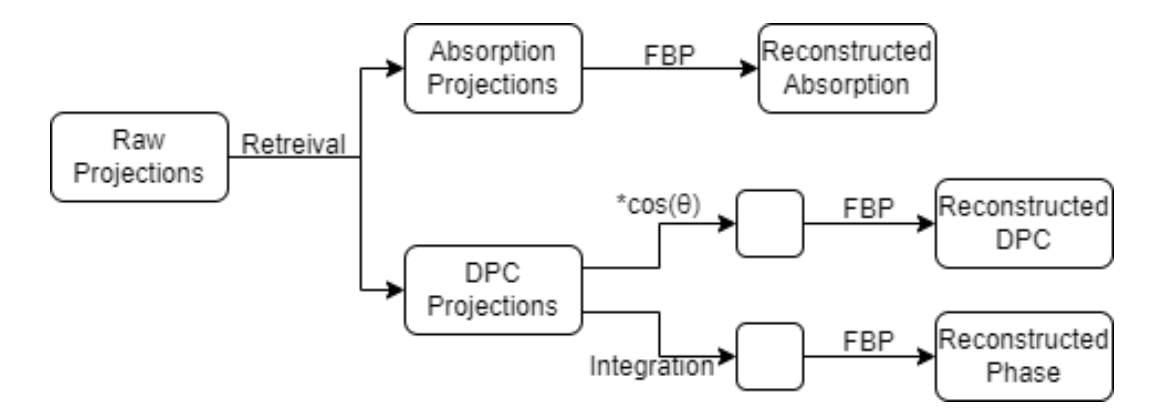


Figure 4: Diagram of CT reconstruction workflow.

# 3. RESULTS AND DISCUSSIONS

The results of the CT reconstruction, including reconstructed attenuation, differential phase contrast (DPC), and phase, are visually presented in Fig. 5. The figure illustrates CT slices in three orthogonal directions passing through the center of the sample. Specifically, the x-z slices traverse through air and water, while the y-z slices traverse through aluminum nitrate and potassium iodide solution.

We could see from the figure that the reconstructed attenuation images exhibit notable contrast between air, PMMA, and the KI solution across all slices. However, discerning between soft materials such as PMMA, water, and aluminum nitrate solution proves challenging, as evidenced by the low contrast profile observed in these regions. Particularly, the water and aluminum nitrate solution appear indistinct in the reconstructed attenuation images, highlighting the limitations of conventional absorption-based x-ray imaging and computed tomography for characterizing soft materials.

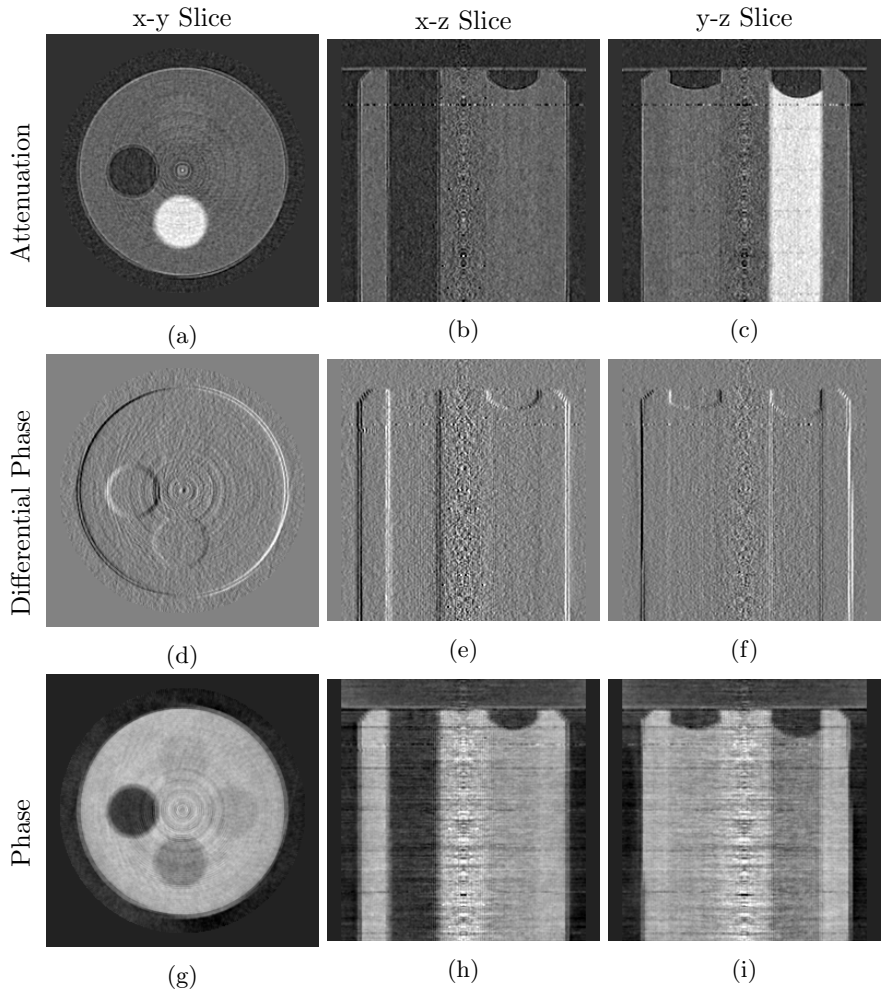


Figure 5: Reconstruction results of single-mask phase contrast CT system. (a-c) Slices from reconstructed attenuation; (d-f) Slices from reconstructed differential phase; (g-i) Slices from reconstructed phase. The x-z and y-z slices pass through the center of the sample.

In contrast, both the Differential Phase Contrast (DPC) image and the Phase image demonstrate significantly heightened contrast levels, particularly for soft materials. Notably, the Phase image effectively distinguishes between these materials, facilitating their clear separation and enhancing overall image clarity. These results underscore the substantial potential of DPC and phase imaging techniques in overcoming the inherent limitations of attenuation-based approaches and improving soft tissue visualization.

Fig. 6 presents a plot of the linear attenuation coefficient ( $\mu$ ) and the decrement of the real part of the refractive index ( $\delta$ ) obtained through multi-contrast CT imaging for different materials. Notably, the plot illustrates that soft materials exhibit similar attenuation properties, as evidenced by their overlapping  $\mu$  values. However, through phase-contrast imaging, these materials can be effectively differentiated based on their distinct  $\delta$  values. This quantitative analysis further corroborates the efficacy of phase contrast in augmenting the diagnostic capabilities of CT imaging, particularly for resolving subtle differences in material composition.

### 4. CONCLUSION

In this study, we have successfully developed an x-ray phase contrast tomography system based on the single-mask phase imaging method. Our system has low demands on x-ray coherence, mask fabrication intricacies, system alignment precision, and detector resolution. This combination of features renders our system both cost-effective and feasible for real-world applications. We will describe the physics models and system design aspects

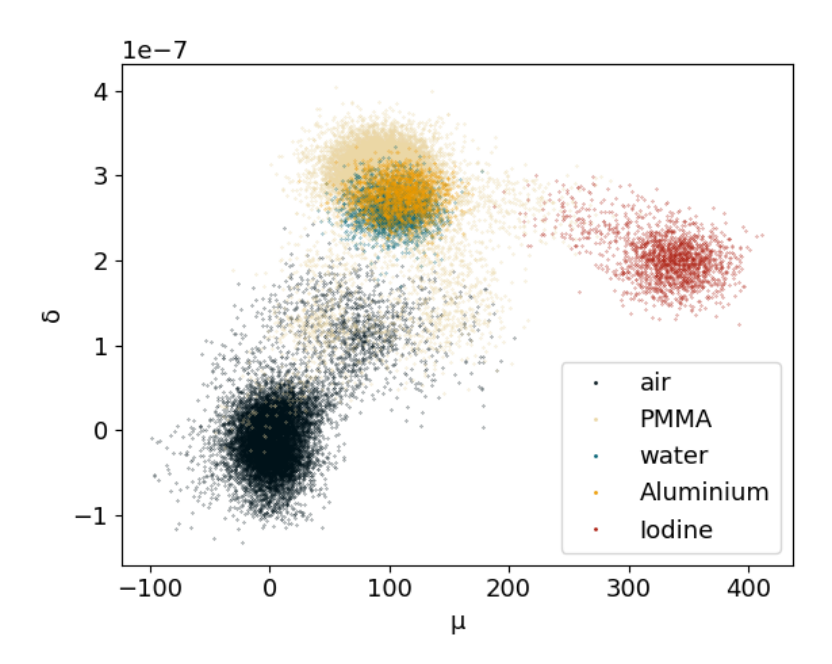


Figure 6: Plot of attenuation coefficient ( $\mu$ ) and  $\delta$  in the refractive index for different materials from the multicontrast CT reconstruction results.

that led to this robust design and multi-contrast image feature at the conference. While we used a spectral detector, spectrosocpic data was not used to obtain these multi-contrast features. The detector was treated as an energy integrating detector with zero dark noise.

Moreover, our system can overcome a persistent challenge prevalent in many previous phase contrast CT systems—sensitivity to temporal system geometry variations induced by factors such as vibrations or fluctuations in temperature. Our imaging system exhibits a heightened resilience towards such geometry fluctuations, underscoring its robustness.

Our phase contrast CT system showcases an exceptional capacity to elevate contrast levels within soft materials. This capability holds substantial promise in the domain of medical imaging, where heightened contrast is essential for improved visualizations of soft tissue structures.

# REFERENCES

- [1] Auweter, S. D., Herzen, J., Willner, M., Grandl, S., Scherer, K., Bamberg, F., Reiser, M. F., Pfeiffer, F., and Hellerhoff, K., "X-ray phase-contrast imaging of the breast—advances towards clinical implementation," *The British Journal of Radiology* 87, 20130606 (Feb. 2014).
- [2] Quenot, L., Bohic, S., and Brun, E., "X-ray Phase Contrast Imaging from Synchrotron to Conventional Sources: A Review of the Existing Techniques for Biological Applications," Applied Sciences 12, 9539 (Jan. 2022).
- [3] Krejci, F., Jakubek, J., and Kroupa, M., "Hard x-ray phase contrast imaging using single absorption grating and hybrid semiconductor pixel detector," *Review of Scientific Instruments* 81, 113702 (Nov. 2010).
- 4] Olivo, A. and Speller, R., "A coded-aperture technique allowing x-ray phase contrast imaging with conventional sources," *Applied Physics Letters* **91**, 074106 (Aug. 2007).
- [5] Olivo, A., "Edge-illumination x-ray phase-contrast imaging," Journal of Physics: Condensed Matter 33, 363002 (July 2021).
- [6] Paganin, D., Mayo, S. C., Gureyev, T. E., Miller, P. R., and Wilkins, S. W., "Simultaneous phase and amplitude extraction from a single defocused image of a homogeneous object," *Journal of Microscopy* 206, 33–40 (Apr. 2002).

- [7] Gürsoy, D. and Das, M., "Single-step absorption and phase retrieval with polychromatic x rays using a spectral detector," *Optics Letters* **38**, 1461 (May 2013).
- [8] Das, M. and Liang, Z., "Spectral x-ray phase contrast imaging for single-shot retrieval of absorption, phase, and differential-phase imagery," *Optics Letters* **39**, 6343 (Nov. 2014).
- [9] Vazquez, I., Harmon, I. E., Luna, J. C. R., and Das, M., "Quantitative phase retrieval with low photon counts using an energy resolving quantum detector," *Journal of the Optical Society of America A* 38, 71 (Jan. 2021).
- [10] Munro, P. R., Ignatyev, K., Speller, R. D., and Olivo, A., "Phase and absorption retrieval using incoherent X-ray sources," *Proceedings of the National Academy of Sciences* **109**, 13922–13927 (Aug. 2012).
- [11] Yuan, J. and Das, M., "Transport-of-Intensity Model for Single-Mask X-ray Differential Phase Contrast Imaging," arXiv:2310.19087 (Oct. 2023).
- [12] Ballabriga, R., Alozy, J., Blaj, G., Campbell, M., Fiederle, M., Frojdh, E., Heijne, E. H. M., Llopart, X., Pichotka, M., Procz, S., Tlustos, L., and Wong, W., "The Medipix3RX: A high resolution, zero dead-time pixel detector readout chip allowing spectroscopic imaging," J. Inst. 8, C02016 (Feb. 2013).
- [13] Das, M., Kandel, B., Park, C. S., and Liang, Z., "Energy calibration of photon counting detectors using x-ray tube potential as a reference for material decomposition applications," in [Medical Imaging 2015: Physics of Medical Imaging], 9412, 263–268, SPIE (Mar. 2015).
- [14] Vespucci, S., Park, C. S., Torrico, R., and Das, M., "Robust Energy Calibration Technique for Photon Counting Spectral Detectors," *IEEE Transactions on Medical Imaging* 38, 968–978 (Apr. 2019).